



ELSEVIER

Journal of Membrane Science 162 (1999) 269–284

**journal of
MEMBRANE
SCIENCE**

A novel ceramic-supported polymer membrane for pervaporation of dilute volatile organic compounds

Jeng-Dung Jou, Wayne Yoshida, Yoram Cohen*

Department of Chemical Engineering, University of California, 5531 Boelter Hall, Los Angeles, CA 90095-1590, USA

Received 29 December 1998; received in revised form 1 April 1999; accepted 19 April 1999

Abstract

A novel asymmetric ceramic-supported polymer (CSP) pervaporation membrane was developed using free-radical graft polymerization of polyvinyl acetate (PVAc) onto a porous tubular silica substrate. The resulting membrane was characterized by pervaporation removal of trichloroethylene (TCE) and chloroform from dilute aqueous solutions. PVAc was chosen since it has a high affinity for TCE and chloroform and a low affinity for water, thus making the membrane permselective toward these solutes. This study has shown, for the first time, that pervaporation is possible even with a large substrate starting pore size (~ 500 Å) and where the active separation phase is a macromolecular layer of terminally anchored chains. Performance of the CSP membrane was assessed at various hydrodynamic conditions and feed concentrations. Resistance of the PVAc/CSP membrane was found to be negligible compared with the concentration boundary layer resistance. The enrichment factor, defined as the ratio of total solute concentration in the permeate to that in the feed, increased with polymer graft yield. For a given graft yield, the enrichment factor approached an asymptotic plateau value, as the tube-side Reynolds number was increased due to increased water flux in response to the rise in transmembrane pressure. Preliminary analysis suggests that the CSP pervaporation membrane performance could be substantially increased by optimizing reaction conditions to produce a higher polymer graft density. © 1999 Elsevier Science B.V. All rights reserved.

Keywords: Ceramic supported polymeric (CSP) membrane; Graft polymerization; Volatile organic compound (VOC) pervaporation; Resistance-in-series model; Membrane surface modification

1. Introduction

In pervaporation, removal of organic components from an aqueous solution is achieved by selective partitioning (solvation) into and diffusion through a polymeric film (i.e. membrane) followed by recovery as condensed vapor on the permeate side. Applications

of pervaporation technology to industrial processes include dehydration of alcohol–water streams [1–10], removal of organic pollutants from dilute aqueous wastes [11–17], separation of close boiling point mixtures [18], and azeotropes [19–21]. To date, most pervaporation studies have involved pure or asymmetric composite polymer membranes with high selectivities. There are, however, well-documented drawbacks which include lack of physical stability and chemical vulnerability to various industrial

*Corresponding author. Fax: +310-206-4107; e-mail: yoram@ucla.edu; <http://www.polysep.ucla.edu>

solvents. Conversely, ceramic membranes are known to have excellent structural integrity and high chemical and thermal resistance [22]; however, these benefits are largely offset by poor selectivity and a limited selection of pore sizes. Such shortcomings can be overcome by surface modification of the ceramic substrate with a polymeric active layer.

Attempts to blend ceramic and polymeric membrane properties have been detailed in the literature. These hybrid membranes have been synthesized by adding ceramic or zeolite particles to the polymer solution prior to casting of a membrane [23,24], dip-coating a porous ceramic substrate in polymer solution [10,25] with subsequent crosslinking [26], and pore-filling of a porous ceramic substrate with acrylamide, followed by cross-linking [27].

A promising approach to active layer formation is the grafting of a covalently bonded polymer surface layer to the porous ceramic substrate. The thin polymer layer provides the desired chemical selectivity and allows controlled reduction of pore size near the membrane surface. To demonstrate the concept of CSP pervaporation membranes, this study focused on the pervaporation removal of trace levels of trichloroethylene (TCE) from aqueous mixtures. Pervaporation of chloroform was also evaluated to investigate the effects of solute diffusivity and to verify pervaporation dependence on the concentration boundary layer resistance. A nonselective silica membrane was grafted with covalently bonded polyvinyl acetate (PVAc) chains using a previously reported method of graft polymerization [28,29]. PVAc polymer was selected as the active membrane phase because of its high solubility with TCE and chloroform. The performance of the PVAc CSP membrane is presented here as a function of hydrodynamic flow conditions and the graft polymer density. These results form the initial basis for future optimization of CSP pervaporation membranes.

2. Analysis

2.1. Resistance-in-series model

Pervaporation can be described by the popular resistance-in-series model or the pore-flow model [30–32]. Although the resistance-in-series model does

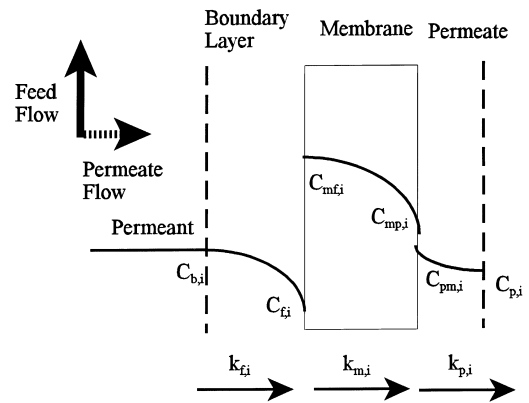


Fig. 1. Schematic of the concentration profile for membrane pervaporation.

not provide a detailed mechanistic description of the pervaporation process, it is convenient for analyzing the relative resistances involved in the process. Briefly, the resistance-in-series model is typically described by three regions as depicted in Fig. 1. Transport of components from the feed solution to the vapor mixture involves several stepwise processes [17]:

1. mass transfer from the feed bulk to the feed-membrane interface;
2. partition of penetrants between feed and membrane;
3. diffusion through the membrane (or membrane layers in the case of a composite); and
4. desorption at the membrane-permeate interface (usually neglected if a high vacuum is maintained on the permeate side).

Based on the above steps, an expression for flux of a given component through the membrane can be derived as

$$J_i = \frac{1}{\frac{1}{k_{f,i}} + \frac{1}{s_{f,i}k_{m,i}} + \frac{1}{(s_{f,i}/s_{p,i})k_{p,i}}} \times \left(C_{b,i} - \frac{s_{f,i}}{s_{p,i}} C_{p,i} \right), \quad (1)$$

where J_i is the molar flux of component i through the boundary layer and $k_{f,i}$, $k_{m,i}$, and $k_{p,i}$ are mass transfer coefficients across tube-side concentration boundary layer, membrane, and permeate film, respectively. $C_{b,i}$ and $C_{p,i}$ are the molar concentrations for the bulk and permeate sides and the partition coefficients $s_{f,i}$ and $s_{p,i}$

are defined as

$$s_{f,i} = \frac{C_{mf,i}}{C_{f,i}}, \quad (2)$$

$$s_{p,i} = \frac{C_{mp,i}}{C_{pm,i}}, \quad (3)$$

where $C_{f,i}$ and $C_{mf,i}$ are the solution/membrane interface concentrations and $C_{mp,i}$ and $C_{pm,i}$ are the membrane/permeate interface concentrations of the solute i , as shown in Fig. 1.

If sufficiently low total pressure is maintained on the permeate side, the permeate concentration and the mass transfer resistance in the permeate film (i.e. $1/k_{p,i}$) [33] may be considered negligible. Therefore, the flux as expressed in Eq. (1) is reduced to

$$J_i = k_{ov,i} C_{b,i}, \quad (4)$$

where $k_{ov,i}$, the overall pervaporation mass transfer coefficient for solute i , is given by

$$\frac{1}{k_{ov,i}} = \frac{1}{k_{f,i}} + \frac{1}{s_{f,i} k_{m,i}}. \quad (5)$$

Diffusive mass flux through the liquid concentration boundary layer on the feed side of the membrane can be expressed as:

$$J_i = k_{f,i} (C_{b,i} - C_{f,i}), \quad (6)$$

where the mass transfer coefficient for transport across the boundary layer, $k_{f,i}$, may be obtained from published Sherwood number correlations. For crossflow pervaporation, these correlations are generally written as

$$Sh = b Re^c Sc^d \left(\frac{d_n}{L} \right)^e, \quad (7)$$

in which $Sh = k_{f,i} d_h / D_i$, $Re = u d_h / \nu$, and $Sc = \nu / D_i$ are the Sherwood, Reynolds, and Schmidt numbers, respectively. D_i is the solute diffusivity in the boundary layer, d_h is the inside diameter of the membrane tube, u the average flow velocity through the tube and ν is the kinematic viscosity. The correlation parameters b , c , d , and e have been reported in the literature for tubular geometry for different flow regimes by various investigators [34–38]. The correlation parameters used for the range of Reynolds numbers in this study were $b=1.62$, $c=0.33$, $d=0.33$, and $e=0.33$ ($Re < 2000$) and $b=1.85$, $c=0.33$, $d=0.33$, and $e=0.33$ ($2000 < Re < 4000$).

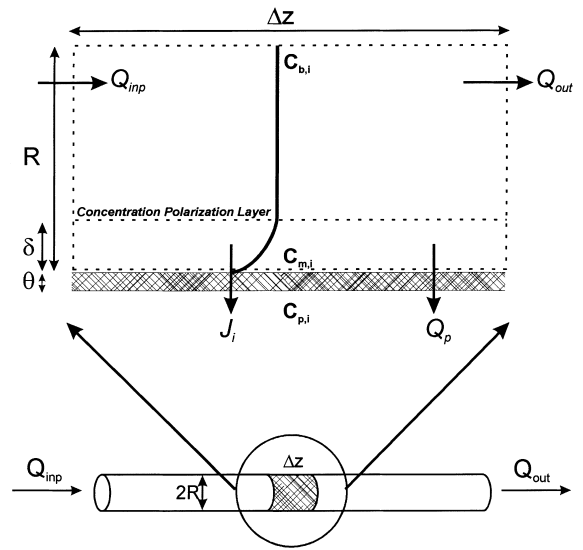


Fig. 2. Schematic representation of transport in the neighborhood and through a pervaporation membrane.

2.2. Solute removal

As a given solute, i , permeates through the membrane, a polarization layer on the liquid side of the membrane is formed. Schematic representation of the polarization phenomenon in a pervaporation process is shown in Fig. 2. In order to derive the relevant mass transfer equation for the time-dependent concentration in the feed reservoir, a number of simplifications can be made for the specific operation of the present membrane system:

1. The thickness of the polarization layer is small compared with the radius of the tube;
2. There is no concentration polarization at the membrane–gas interface (i.e. the permeate side is maintained at essentially zero solute partial pressure);
3. The mass transfer resistance in the permeate film on the shell-side, $1/k_{p,i}$, and the permeate concentration can be considered to be negligible due to the high vacuum maintained on the permeate side (e.g. < 10 Torr);
4. The solute convective flux through the membrane is negligible relative to the solute diffusive flux (i.e. the radial Peclet number, Pe_r , is small compared with unity); and finally
5. We also note that in the present membrane system, axial pressure drop is negligible (e.g. the pressure

between inlet and outlet of the membrane was less than 1%).

Thus, the transmembrane flux can be approximated to be constant along the length of the membrane.

Following the above simplifications the relationship between inlet and outlet concentrations of the membrane can be derived from a component mass balance on a differential element along the membrane (Fig. 2)

$$\frac{d(QC_{b,i})}{dz} = 2\pi RJ_i, \quad (8)$$

where J_i is given by Eq. (6). As a result of simplification (5) above, $dQ/dz = -Q_p/L$, where Q_p is the total permeate flow rate and L is the length of the membrane tube. Subsequent integration of Eq. (8), from the membrane tube entrance to the exit, leads to the following expression for the solute concentration at the exit of the membrane tube

$$C_{i,out} = C_{i,inp} \left(1 - \frac{Q_p}{Q_{inp}}\right)^{\left(\frac{2\pi RK_{ov,i}L}{Q_p}\right)}, \quad (9)$$

where $C_{i,inp}$ and $C_{i,out}$ are the concentrations of i at the inlet and outlet of the membrane, Q_{inp} the feed flow rate at the inlet to the membrane, and R is the inside radius of the membrane tube.

An overall solute balance on the feed reservoir (Fig. 3) leads to

$$V \frac{dC_{i,inp}}{dt} = [(Q_{inp} - Q_p)C_{i,out} - Q_{inp}C_{i,inp}], \quad (10)$$

which in combination with Eq. (9) leads to the following expression for the solute concentration decline in the feed reservoir:

$$C_{i,inp} = C_{i,0} \left(\frac{V_0}{V_0 - Q_p t}\right)^{\frac{S}{Q_p}}, \quad (11)$$

where

$$S = (Q_{inp} - Q_p) \left(1 - \frac{Q_p}{Q_{inp}}\right)^{\left(\frac{k_{ov,i}A}{Q_p}\right)} - Q_{inp}, \quad (12)$$

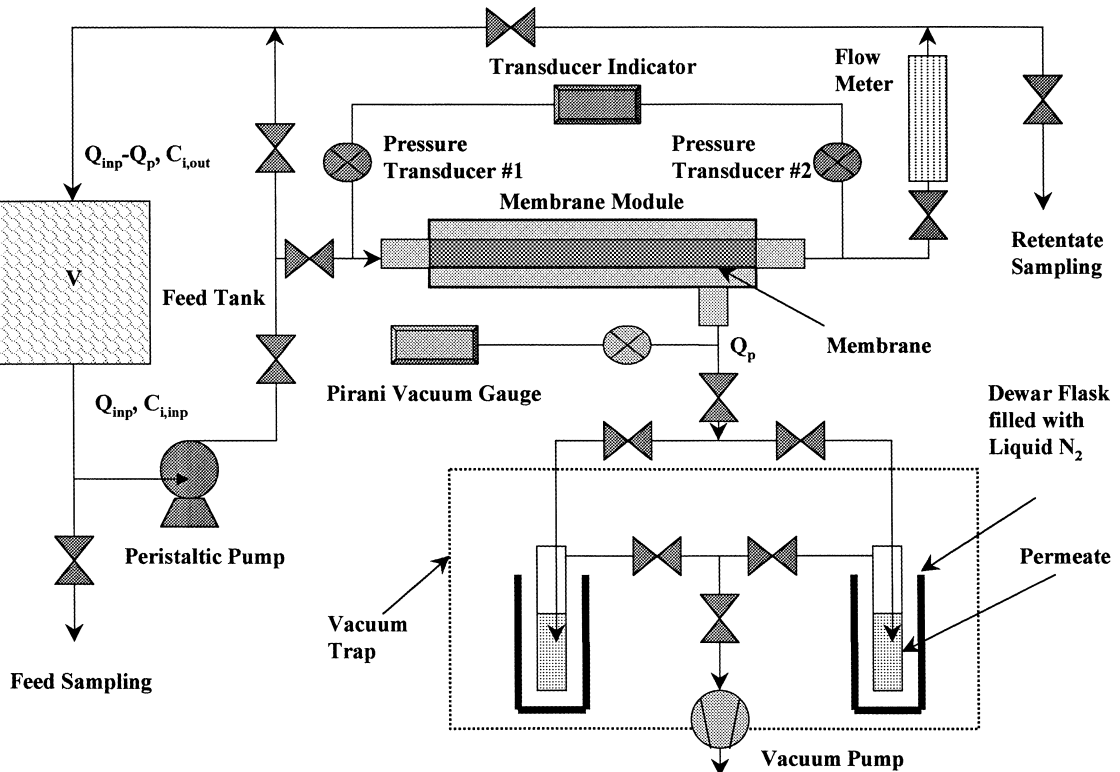


Fig. 3. Pervaporation system.

in which $C_{i,\text{inp}}$ is the feed concentration at operation time t , $C_{i,0}$ the initial feed concentration, and V_0 is the initial volume of the solution in the feed reservoir. When the permeate flow is assumed to be very small, such that $Q_p/Q_{\text{inp}} \ll 1$, Eq. (9) can be reduced to a more familiar exponential relationship, $C_{i,\text{out}} = C_{i,\text{inp}} \exp[2\pi RLk_{\text{ov}}/Q_{\text{inp}}]$. Consistent with the above approximation, when $Q_p t/V_0 \ll 1$, one can show that Eq. (11) reduces to $\ln(C_{i,\text{inp}}/C_{i,o}) = -(S/V_0)t$, which indicates an exponential decline of the solute concentration in the feed reservoir.

The overall mass transfer coefficient $k_{\text{ov},i}$ can be determined from experimental pervaporation data by Eq. (11) and the boundary-layer mass transfer coefficient $k_{f,i}$ for the membrane can be obtained from Eq. (7). This allows the calculation of $1/s_{f,i} k_{m,i}$, the contribution of membrane resistance to the overall mass transfer coefficient, delineated by the third term in Eq. (5). It is noted that if the membrane/solute partition coefficient is large (i.e. when the solute=s affinity for the membrane is high) the membrane resistance term is expected to be much smaller than the liquid boundary-layer resistance on the tube-side of the membrane.

3. Experimental

3.1. Materials

The inorganic substrate for the CSP membranes was porous silica in a tubular configuration, 19 cm in length and 0.4 mm in thickness, with a pore size of 500 Å and surface area of 45.5 m²/g. The silica membrane was supplied by the Industrial Research Institute of Miyazaki, Tsunehisa, Japan. Surface activation was achieved using a solution of vinyl trimethylsilane (98% pure, Aldrich, Milwaukee, WI) and reagent-grade xylene solvent (Fisher Scientific, Tustin, CA).

The polyvinyl acetate (PVAc) surface layer was synthesized by graft polymerization using reagent grade vinyl acetate monomer (Fisher Scientific, Tustin, CA) in ACS-grade ethyl acetate solvent (Fisher Scientific, Tustin, CA). The free radical initiator used for graft polymerization was α,α' -azobis(2,4-dimethylvaleronitrile) purchased from Dupont (Wilmington, DE).

3.2. Membrane synthesis

Membrane selectivity is dependent mainly on preferential solubility of the permeating species in the active polymer layer. In order to choose a polymer with maximum selectivity, the Hansen solubility parameter approach was used. In this approach, the relative affinity of any permeating species to a given polymer can be ranked using three solubility parameters: δ_d , δ_p , and δ_h . These three parameters represent nonpolar, polar, and hydrogen bonding interactions that can be predicted using available polymer/permeate group contributions [39]. Typically, the solubility parameters are plotted orthogonally as axes on a three-dimensional graph, producing a single point in the Hansen solubility parameter space for each polymer and permeate. An illustration of the Hansen solubility parameter map for a selected group of polymers and solvents is shown in Fig. 4. For a given solvent, the distance from the polymers in Fig. 4 is proportional to the quality of the solvent for the polymer. As the distance between the solvent and polymer decreases, the quality of the solvent for the polymer increases [40]. Out of the various polymers investigated, PVAc ($\delta_d=15.2$, $\delta_p=11.5$, and $\delta_h=7.6$ (J/cm³)^{1/2}) was chosen for TCE ($\delta_d=14.5$, $\delta_p=13.1$, and $\delta_h=5.3$ (J/cm³)^{1/2}) and chloroform ($\delta_d=11.0$, $\delta_p=13.7$, and $\delta_h=6.3$ (J/cm³)^{1/2}) pervaporation because its close proximity to these solvents in the Hansen solubility parameter space indicates a high affinity for those chemicals [41,42].

Surface modification of the support membrane was performed in three steps: pretreatment, surface activation, and graft polymerization. The silica substrate was first treated with a 2% aqueous HCl solution to clean the substrate and to fully hydroxylate the surface. In the surface activation step, the hydroxyl groups were replaced with a silyl group by means of an anhydrous silylation reaction using vinyl trimethoxysilane [28,41–43]. This silylation step produced covalently bonded vinyl groups necessary for the polymerization step. Finally, PVAc was grafted to the surface using vinyl acetate as a monomer and ethyl acetate as a solvent. The graft polymerization procedure followed the method of Browne et al. [29] adapted for a tubular membrane support [42]. Using the above modification procedure PVAc graft yields ranged from 0.17 to 0.43 mg/m²

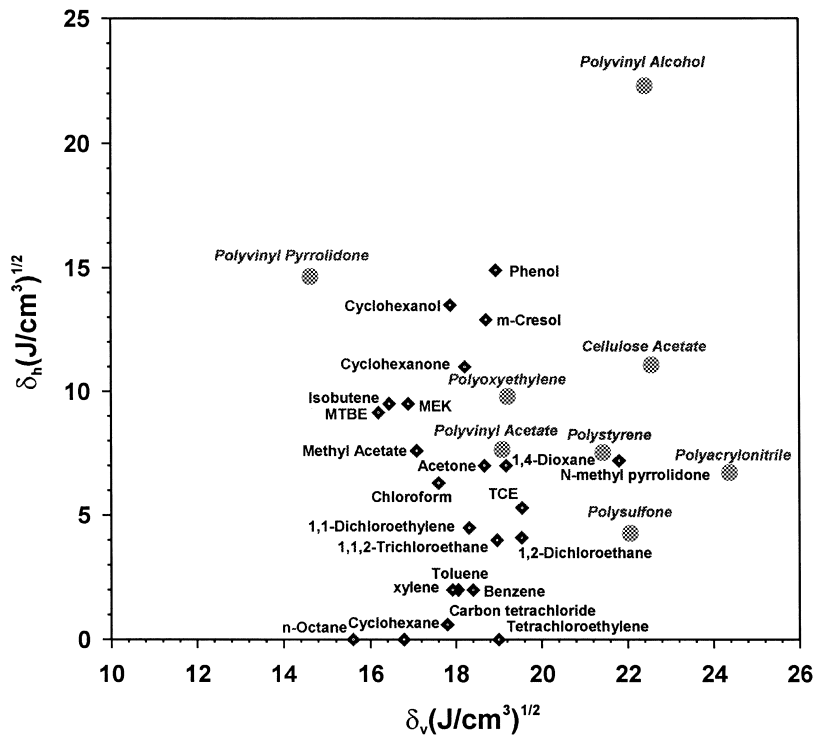


Fig. 4. Hansen space solubility parameter map. Hansen space solubility parameters, δ_d , δ_p , and δ_h , represent nonpolar, polar, and hydrogen bonding interactions and $\delta_v = (\delta_d^2 + \delta_p^2)^{1/2}$.

total surface area of the porous silica support membrane.

It is emphasized that the CSP membrane is modified with a polymer layer which is grafted onto the tube-side surface of the porous support. This active polymeric membrane phase consists of a layer of terminally anchored chains. It is interesting to note that previous studies on membrane pore-filling graft polymerization reported significantly higher graft yields [46–49]. For example, Yamaguchi et al. [46] reported poly(methyl acrylate) graft yields in excess of 20 000 mg/m² for the modification of a polyethylene membrane. As apparent from reported TEM images for the above membranes, this latter modification method results in the formation of both surface grafted chains and pore-filled homopolymer throughout the membrane pore space. It appears that the membrane's original thickness increased by a factor of about 1.5. It is emphasized that the CSP membrane is produced by a different process which results in a single layer of tethered chains covalently bonded to the substrate

surface. Therefore, for the CSP membrane the area-specific polymer graft yield, as expected, is lower than for the pore-filling graft polymerization modification.

3.3. Pervaporation experimental procedures

Pervaporation of dilute aqueous TCE solutions through the PVAc/silica membranes was carried out experimentally using a bench-scale apparatus schematically depicted in Fig. 3. Since TCE is a volatile organic solvent, special precautions were necessary to prevent uncontrolled volatilization. A tedlar bag (Chromatography Research Supplies, Addison, IL) containing approximately 1000 ml of feed solution was used as a reservoir in order to eliminate TCE loss by volatilization. Feed solution was pumped through the tube-side of the module and the retentate was recycled back to the feed tank with the flow rate measured by an on-line flow meter. The gaseous permeate was condensed and collected by means of two vacuum traps immersed in liquid nitrogen. Low

pressure, approximately 2 Torr on the permeate side, was maintained by a vacuum pump (Model M8C, Fisher Scientific, Pittsburgh, PA). Transmembrane pressure was measured by pressure transducers (Model CD 223, Validyne, Northridge, CA) and a vacuum gauge (Pirani Vacuum Gauges, Edwards, Wilmington, MA) placed on the feed and permeate sides of the membrane, respectively. All pervaporation experiments were conducted at room temperature.

Prior to the pervaporation tests, a blank experiment was conducted by pumping a TCE solution through the entire flow system but bypassing the membrane. The feed was then periodically checked to verify that there was no decline in TCE concentration. This test was carried out to detect any possible TCE losses by adsorption or permeation through the system components. After the blank test demonstrated that there were no volatilization losses or leaks, the feed bag was filled with the TCE solution and connected to the system. The vacuum pump on the permeate side was turned on for half-an-hour before the start of actual data collection to evacuate any remaining air from the system. The permeation rate was then determined by monitoring the volume of condensed permeate in the dewar flasks throughout the course of the experiment.

Samples were taken at 30 min intervals and were analyzed immediately following withdrawal from the feed bag. TCE analysis was carried out using a gas chromatograph (Hewlett-Packard 5890A) equipped with a flame ionization detector, using a $6' \times 1/8''$ stainless steel column packed with Carbowax Graphitized Carbon Black 2AC (Alltech, Deerfield, IL) for halocarbons analysis.

4. Results and discussion

4.1. Hydraulic water permeability

Prior to pervaporation tests, the silica membranes were characterized by hydraulic permeability measurements with water. A series of measurements were performed with the unmodified, silylated and grafted silica membranes. The silica membrane supports were modified with the goal of attaining a level of pore reduction sufficient for pervaporation. The average hydraulic permeability, based on dead-end filtration measurements for seven different unmodified 500 Å

silica membrane, was $1.184 \times 10^{-15} \text{ cm}^2$ with less than 15% deviation.

The silylated silica membranes were impermeable to water up to a transmembrane pressure of 12 psia, indicating that the membrane had become hydrophobic. The silylated membranes were subsequently modified by vinyl acetate graft polymerization. Mild reaction conditions (i.e., 10% or 25% monomer concentration and 60°C or 70°C reaction temperature) were employed to increase the contribution of graft polymerization to the growth of surface chains, while limiting the effect of polymer grafting [41,42,44]. Once grafted, the CSP membranes, like the silylated membranes, exhibited negligible water permeability up to a transmembrane pressure of 12 psia. Negligible hydraulic water permeability for the CSP membrane, as our experience has shown, is a prerequisite for a suitable pervaporation membrane.

4.2. Pervaporation permeate flux

Tubular modified membranes were also characterized by measuring pervaporation permeate flux using the apparatus shown in Fig. 3. The permeate flux ranged from 0.32 to 0.64 l/h m² which is about one order of magnitude higher than is commonly expected for pervaporation membranes. This range of permeate flux suggests a relatively open pore structure. Therefore, the permeate flux should decrease with increasing polymer graft yield.

The permeate flux is expected to depend upon the polymer configuration in the membrane pores, which is in turn affected by solvent properties. To assess the above possibility, the permeate fluxes for TCE/water solution (Table 1) and pure water were measured under identical pervaporation conditions, at a fixed Reynolds number of 610. The presence of TCE in the aqueous solution decreased the permeate fluxes by about 2% for the low graft polymer density membrane (0.17 mg/m²) and 6% for high graft polymer density membrane (0.43 mg/m²), when compared to the original pure water pervaporation permeate flux. These results support the argument that TCE, a solvent with high affinity for PVAc, causes the terminally-grafted PVAc chains to swell, thus occupying a greater portion of the membrane pore volume compared to the volume occupied during exposure to pure water. In other words, the solvent causes surface chains to extend

Table 1
Summary of TCE pervaporation results for silylated and PVAc-grafted ceramic membranes

Graft yield (mg/m ²)	Silylation coverage (mg/m ²)	Feed flow rate (ml/min)	Re	Permeate flux (l/h m ²)	C _{0,TCE} (ppm)	k _{f, TCE} ^a (cm/s)	K _{M, TCE} ^b (k _M =S _f ×k _m) (cm/s)	β ^c
0.17	0.69	120	610	0.439 (0.448) ^d	641	8.353×10 ⁻⁴	Negligible	69
0.17	0.69	170	860	0.474	68	9.372×10 ⁻⁴	Negligible	71
0.17	0.69	170	860	0.474	600	9.372×10 ⁻⁴	Negligible	71
0.17	0.69	300	1260	0.518	653	1.064×10 ⁻³	Negligible	75
0.17	0.69	550	2780	0.642	554	1.381×10 ⁻³	Negligible	78
0.38	0.45	120	610	0.359	681	8.353×10 ⁻⁴	Negligible	86
0.43	0.66	120	610	0.319 (0.340) ^d	638	8.353×10 ⁻⁴	Negligible	102
0.43	0.66	300	1260	0.366	457	1.064×10 ⁻³	Negligible	106
–	0.69	120	610	0.439	550	8.353×10 ⁻⁴	5.753×10 ⁻³	65
–	0.69	170	860	0.474	591	9.372×10 ⁻⁴	5.753×10 ⁻³	66

^a Determined by Eq. (11).

^b Determined by Eq. (5).

^c Enrichment factor, $\beta=C_{\text{permeate}}/C_{\text{feed}}$.

^d Permeate flux was determined by pervaporation experiments at same flow conditions only with pure water.

away from the surface of the silica membrane pores, thereby decreasing the effective pore radius and reducing permeate flow through the membrane. Therefore, lower permeate flux should be expected with increasing polymer graft yield (Table 1).

4.3. Pervaporation of TCE/water and chloroform/water binary mixtures

The membrane active separation layer must be selected so as to maximize the affinity of the organic solute for the polymer active phase. This especially important since water molecules are small in comparison with most volatile organic molecules. According to the Hansen solubility parameter approach, PVAc exhibits good organophilicity for both TCE and chloroform and is thus an ideal pervaporation separation phase for these chemicals [41,42]. Based on this selectivity, PVAc-silica membranes were synthesized for pervaporation studies of the TCE/water and chloroform/water systems.

Results of pervaporation experiments for TCE removal with the PVAc/silica membrane, for different tube-side Reynolds numbers, are shown in Fig. 5 (PVAc-grafted CSP membrane: graft yield=0.17 mg/m²). The results clearly show that TCE is removed more efficiently as the tube-side Reynolds number is increased. This is not surprising since the tube-side mass transfer coefficient also increases with increasing tube-side Reynolds numbers (Table 1).

Indeed, the mass transfer coefficients for this concentration boundary layer controlled transport, obtained from Eq. (7) with the correlation parameters reported by Lipski and Côté [37] and Karlsson and Tragardh [38], closely match the experimentally determined overall mass transfer coefficients (Eq. (9)). The data obtained over the range of Reynolds numbers studied indicate that membrane resistance for TCE transport is negligible relative to the tube-side boundary-layer resistance.

In order to demonstrate the concentration independence of the overall mass transfer resistance, a perva-

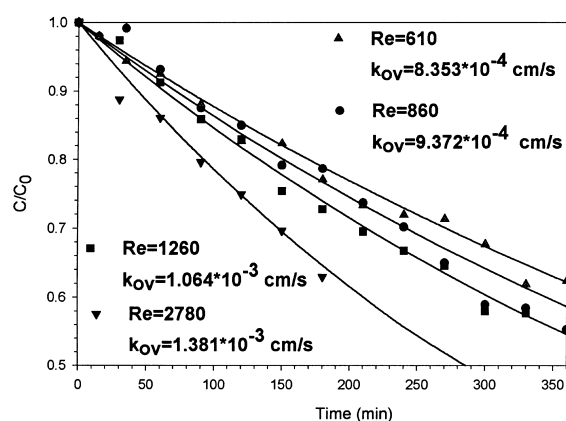


Fig. 5. Relative concentration-time data for pervaporation. (PVAc-grafted membrane: graft polymer density=0.17 mg/m², C₀ initial feed concentration=500–700 ppm). Solid lines represent theoretical predictions Eqs. (11) and (7) for the mass transfer coefficient.

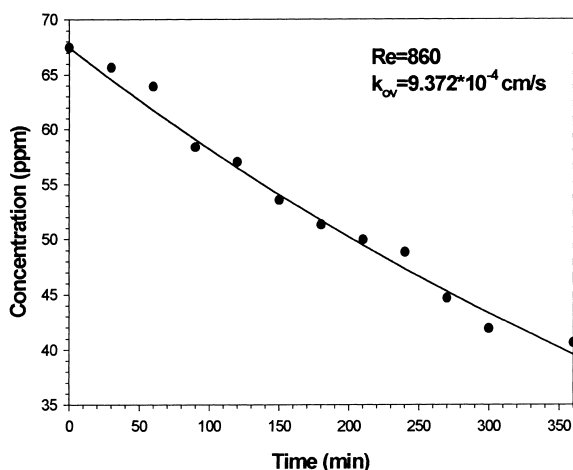


Fig. 6. TCE concentration in the feed reservoir: low concentration regime. (PVAc-grafted membrane: graft polymer density=0.17 mg/m²). Solid lines represent theoretical predictions Eqs. (11) and (7) for the mass transfer coefficient.

poration experiment using a PVAc modified CSP membrane of 0.17 mg/m² graft yield was conducted with initial feed concentration of 68 ppm (relative to >500 ppm initial concentration shown in Fig. 5), and a feed flow rate of 170 ml/min ($Re=860$). The overall mass transfer coefficient for this pervaporation experiment (Fig. 6) was identical to that obtained for a higher concentration using the same flow conditions (Fig. 5). These results confirm that the performance of the PVAc-silica membrane for TCE pervaporation was independent of concentration over the range 30–700 ppm.

A comparison of the removal of TCE using silylated and PVAc membranes is shown in Fig. 7. The overall mass transfer coefficient for the silylated membrane was lower than for the PVAc CSP membrane over the range of Reynolds numbers studied (see Fig. 8). These results indicate the presence of a non-negligible TCE mass transfer resistance in silylated membranes (see Table 1). It is interesting to note that the total permeate flux for the silylated membrane, over the range of Reynolds numbers studied, was nearly identical to the PVAc grafted membrane at the same Reynolds number. Unlike the grafted membranes, however the silylated membrane exhibited significant membrane resistance, possibly due to the low affinity of TCE for surface vinylsilane groups.

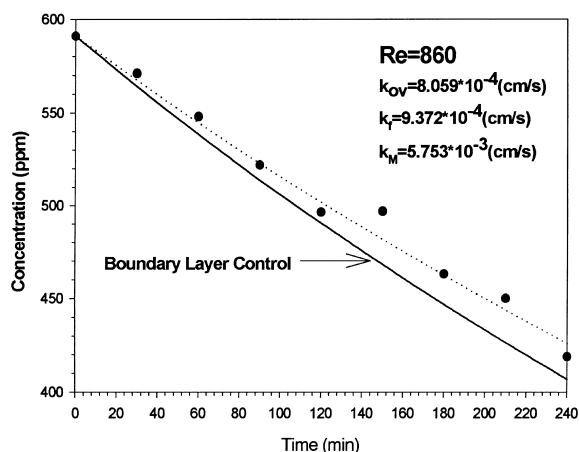


Fig. 7. TCE concentration in the feed reservoir. (Silylated silica membrane). Solid lines represent theoretical predictions Eqs. (11) and (7) for the mass transfer coefficient.

Chloroform was chosen as a second organic target solute to confirm the dominance of the tube-side boundary-layer mass transfer resistance. The separation distances between chloroform and polyvinyl acetate ($\Delta=4.87 \text{ (J/cm}^3)^{1/2}$) and TCE and polyvinyl acetate ($\Delta=2.89 \text{ (J/cm}^3)^{1/2}$) on the Hansen solubility parameter map (Fig. 4) are both in the range ($\Delta < 5$) indicating high solute–polymer affinity [39]. However, the diffusivity of chloroform in water is about 18% higher than for TCE at the experimental pervaporation temperature of 25°C. Therefore, the

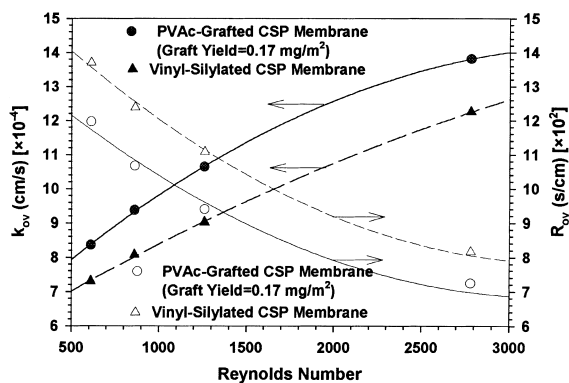


Fig. 8. Overall mass transfer coefficients and overall resistance for PVAc-grafted and vinyl-silylated (CSP) membranes. R_{ov} (Overall resistance)= $1/k_{ov}$. Solid lines represent theoretical predictions for the mass transfer coefficient Eq. (7).

Table 2
Effects of solute diffusivity in water on pervaporation for a PVAc/silica CSP membrane

Reynolds number	TCE		Chloroform	
	k_{TCE} (cm/s)	β_{TCE}	$k_{chloroform}$ (cm/s)	$\beta_{chloroform}$
610	8.353×10^{-4}	102	9.353×10^{-4}	114
1260	1.064×10^{-4}	106	1.191×10^{-4}	118

PVAc-grafted CSP membrane: graft density=0.43 mg/m².
 $D_{TCE}=9.135 \times 10^{-6}$ cm²/s @ 25°C, $D_{chloroform}=1.081 \times 10^{-5}$ cm²/s @ 25°C.
 $\delta_{TCE} \approx \delta_{chloroform}$.
 $k_{ov,i}^{\infty} (D_i^{0.67})$.

enrichment of chloroform in the permeate should be higher relative to TCE at the same experimental conditions. This behavior is illustrated for two different Reynolds numbers in Table 2. We note that the ratio of the TCE to chloroform diffusivity (in water) raised to the 0.67 power ($(D_{TCE}/D_{chloroform})^{0.67} \approx 0.893$) accounts for the difference in the solute pervaporation flux for these two compounds. This observation also supports the conclusion that the concentration boundary-layer resistance is the dominant resistance to pervaporation.

The TCE enrichment factor, β ($=C_{p,i}/C_{b,i}$), for PVAc-silica and silylated-silica membranes, which was in the range 65–106, was found to increase with the tube-side Reynolds number as a consequence of the reduction in the concentration boundary-layer resistance with increasing Reynolds number (Figs. 8 and 9). The higher enrichment factor for PVAc-silica membranes is attributed to the negligible membrane resistance. As discussed earlier, the enrichment of the

solute in the permeate stream is controlled solely by the tube-side boundary layer resistance to mass transfer.

The enrichment factor appears to approach an asymptotic value with increasing Reynolds number, even though the overall mass transfer coefficient increases (Figs. 8 and 9). This behavior is linked to the increase in water flux in response to the unavoidable rise in transmembrane pressure with increasing tube-side Reynolds number. The analysis of water permeation and the design approach to increasing the enrichment factor are addressed in the following section.

4.4. Effect of graft polymer density on enrichment factor and permeate flux

The enrichment factor, β , and the commonly used membrane separation factor, α , are related through the following expression:

$$\alpha = \frac{x_{p,i}/x_{p,j}}{x_{f,i}/x_{f,j}} = \beta \frac{(1 - x_{f,i})}{(1 - x_{p,i})}, \quad (13)$$

$$\beta = \frac{x_{p,o}}{x_{b,o}}, \quad (14)$$

where $x_{p,i}$ and $x_{p,j}$ are the mole fractions of species i and j in the permeate and $x_{f,i}$ and $x_{f,j}$ the corresponding mole fractions of i and j in the feed, $x_{p,o}$ the mole fraction of organic in the permeate and $x_{b,o}$ is the mole fraction of organic in the feed. We note that for an dilute solution of i , $\alpha = \beta$ provided that $x_{f,i}$, $x_{p,i} \ll 1$.

The enrichment factor in Eq. (14) can be expressed as

$$\beta = \frac{J_o / (J_o + J_w)}{(C_{b,o} / C_{T,feed})}, \quad (15)$$

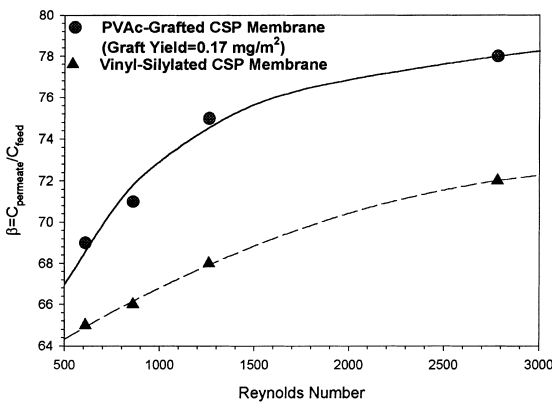


Fig. 9. Enrichment factors for PVAc-grafted and vinyl-silylated (CSP) membranes.

in which J_o is the pervaporation molar flux of organic component, J_w the pervaporation molar flux of water, $C_{b,o}$ the molar bulk feed concentration of the organic component, and $C_{T,feed}$ is the total molar feed concentration including all species. The organic permeation flux in the present CSP pervaporation membranes is given by Eq. (4), and substitution of this expression into Eq. (15) results in:

$$\beta = \frac{k_{ov} C_{T,feed}}{k_{ov} C_{b,o} + J_w} \quad (16)$$

For a given feed flow rate (i.e., a fixed tube-side Reynolds number) and concentration, the enrichment factor is controlled by the water flux J_w . Eq. (16) indicates that, for the CSP membrane, pervaporation performance will increase with decreasing water flux. As a first step, however, the membrane must not allow the convection of liquid water. The unmodified membranes used in the present study could not fulfill this requirement due to excess liquid water permeability under pervaporation conditions. However, once the membrane was modified, the polymeric phase served to prevent liquid water permeation through the membrane and to also increase the membrane resistance to water vapor permeation.

In the absence of the polymeric layer, and in the hypothetical case in which bulk water permeation can be restricted by the support membrane, water pervaporation flux, which is controlled by diffusion resistance of the support, can be approximated by

$$J_w = (D_w \varepsilon / \theta \tau) P_w^s / RT, \quad (17)$$

where D_w is the diffusivity of water vapor ($0.197 \text{ cm}^2/\text{s}$) at the permeate side which is at pressure of 2 Torr, τ the tortuosity, taken to be 1.5, ε the membrane porosity of 0.7, θ the membrane thickness of 0.04 cm, T the temperature, P_w^s the water saturation pressure at temperature T , and R is the universal gas constant. For example, the flux of water vapor through the membrane at 298 K, which occurs via Knudsen diffusion through the porous support, as calculated from Eq. (17) and expressed in terms of liquid water flux is 1.83 l/h m^2 in comparison with the experimentally measured water flux of 0.42 l/h m^2 for the CSP membrane at Re 610. Clearly, the grafted polymer layer which serves as a resistance to liquid water permeation reduces water flux through the membrane. We emphasize that in reality, without the polymer phase, perva-

poration is not possible with the unmodified support due to permeation of liquid water. Water flux reduction for the current CSP membranes results in enrichment factors one to two orders of magnitude lower than those theoretically predicted for equilibrium binary distillation, although distillation separation is achieved at a much higher energy cost. In order to identify an approach to improving performance of future CSP pervaporation membranes, it is useful to explore the effect of transmembrane pressure and the graft yield on the pervaporation process.

At a given tube-side Reynolds number, increasing polymer graft yield caused an increase in enrichment factor and a decrease in total flux. For example, over the range of Reynolds numbers 600–3000, the total permeate flux decreased by up to 30% as the graft yield increased from 0.17 to 0.43 mg/m^2 (Table 1). As the grafted polymer phase density increased, water flux through the membrane decreased due to a reduction in the effective pore diameter for water permeation. At the same time, TCE flux through the membrane was maintained, since the tube-side concentration boundary layer resistance dominated the resistance to TCE transport. With increasing tube-side Reynolds numbers, TCE flux increased as the tube-side mass transfer coefficient increased, although water flux was also observed to increase. In the present membrane system, as the transmembrane pressure increases, with increasing tube-side Reynolds number, so did the flux of water through the membrane. In accordance with the above behavior, pervaporation transport through the CSP membranes can be approximated in terms of a linear combination of convective and diffusive transport given by the following expression:

$$N_p = \frac{Q_p}{A} = \frac{k \Delta P}{\mu \theta} + \sum_{i=1}^m k_{ov,i} \frac{M_i}{\rho_i} \Delta C_i = \frac{\Delta P}{R_c} + \sum \frac{\Delta C_i}{R_i}, \quad (18)$$

where N_p is the total permeate flux (l of water/ m^2 h) and A is the active area of the membrane. The first term on the right-hand side represents the total convective flux as described by Darcy's law where k is the permeability for the bulk solution permeating through the open pore space, ΔP the transmembrane pressure, μ the solution viscosity and θ is the thickness of the membrane. The second term on the right-hand side of Eq. (18) represents the sum of m component fluxes

due to diffusion where k_i is the overall mass transfer coefficient of species i , ΔC_i the difference between the feed and permeate side concentrations for species i , M_i the molecular weight of species i and ρ_i is the density of species i . For convenience it is useful to define an overall resistance to convective flux, $R_c = \mu\theta/k$ and an overall diffusive resistance for each component, $R_d = (\rho_i/M_i)/k_i$. In order to evaluate the permeation characteristics of the membrane, pervaporation experiments can be performed with pure water as the sole permeant. Under such conditions, Eq. (18) may be reduced to the following equation:

$$N_w = \frac{Q_w}{A} = \frac{\Delta P}{R_c} + \frac{\Delta C_w}{R_d}, \quad (19)$$

in which N_w is the volumetric water permeation flux (i.e., $N_w = J_w M_w / \rho_w$) and ΔP_w is the transmembrane pressure. Under reasonably high steady-state vacuum on the permeate side, the permeate concentration is nearly zero and ΔC_w , the concentration driving force for water, may be assumed to be a constant approximately equal to the saturation vapor pressure of water at the feed temperature; R_c the transport resistance for water convection through the membrane and R_d is the overall resistance to diffusive transport. It is expected that the resistances R_c and R_d will increase with polymer graft yield due to increased polymer volume fraction in the membrane pores. Since the second term in Eq. (19) represents diffusive transport which is not

expected to be a function of transmembrane pressure, for the normal range of pervaporation conditions, it should remain constant for a given temperature and polymer graft density. Therefore, both R_c and R_d can be determined by plotting the pervaporation water flux, N_w , versus transmembrane pressure ΔP_w , if the relationship between pure water flux and transmembrane pressure is linear as described by Eq. (19). The intercept of such a plot represents the diffusion term $\Delta C_w/R_d$. In other words, pure diffusive transport of water will only occur when the transmembrane pressure is negligible such that $\Delta P/R_c \rightarrow 0$. Clearly, this situation will not occur when the permeate side is under vacuum. In principle, it is possible to operate under a vanishing transmembrane pressure condition by using sweep gas to keep the partial pressure of the permeating component sufficiently low.

The above analysis is illustrated in Fig. 10 for two different membranes each with a different graft yield. As the graft yield increased from 0.17 to 0.43 mg/m², the resistance to water transport by convection (R_c) and diffusion (R_d) increased by 44% and 33%, respectively. Correspondingly, the diffusive permeation flux of water decreased by about 24%. It is noted, as discussed earlier, that the permeation flux of the organic solute is only slightly affected by the change in water permeation flux. Water flux, in turn is reduced with increased polymer graft yield. Therefore, it follows that in order to increase the membrane selectivity

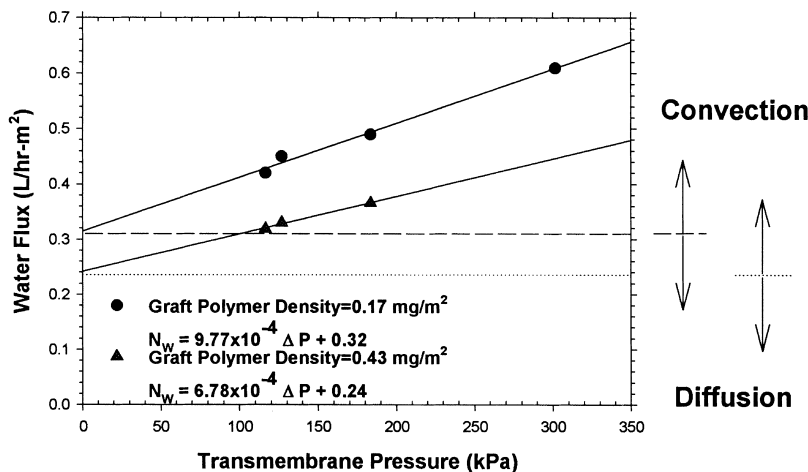


Fig. 10. Water flux versus transmembrane pressure.

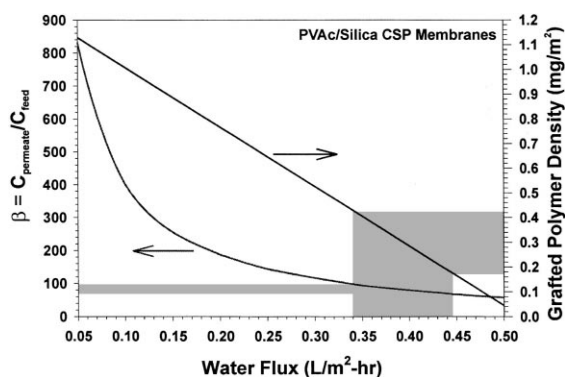


Fig. 11. Design curve for CSP membrane pervaporation. (PVAc/Silica CSP membranes).

for the organic solute, a higher polymer graft density and possibly a smaller starting pore size for the ceramic membrane support are required.

4.5. Membrane optimization

It is important to note that N_w represents the contribution of both diffusive and pressure-driven transport (Eq. (19)). For the present CSP membranes it was found that the water flux decreased linearly with increasing polymer graft yield, a result consistent with the study of Castro et al. [45]. For a given membrane substrate, feed concentration, and tube-side Reynolds number, a relationship between β and the graft polymer density can be constructed as illustrated in Fig. 11. The shaded area in Fig. 11 represents graft polymer density of current CSP membranes; according to this example design curve, increasing the graft polymer density from our current highest value of 0.43 to 1.15 mg/m^2 would increase the achievable enrichment factor from 100 to 800. Such a level of graft yield is feasible with the present method of graft polymerization [28,29]. Higher graft polymer densities can be obtained by careful optimization of surface activation and graft polymerization conditions. Current research is ongoing to increase polymer graft density and elucidate the relationship between graft polymer surface characteristics and membrane performance.

5. Conclusion

A novel ceramic-supported polymeric (CSP) pervaporation membrane was developed wherein the

positive attributes of pure polymeric and ceramic membranes have been combined into an asymmetric composite that is both chemically and physically stable. These membranes can be tailored for a variety of separation applications through a proper selection of the graft polymer phase and optimizing polymerization conditions.

The active separation layer in these membranes consists of a thin macromolecular layer of terminally anchored polymer chains. For the range of Reynolds numbers studied, membrane performance for the separation of volatile solvents such as TCE and chloroform from aqueous solutions is limited only by the feed-side concentration boundary layer. The enrichment factor for separation of TCE and chloroform from water varied from 69 to 106. It was also found that the enrichment factor increased with increasing polymer graft yield. Moreover, membrane pervaporation performance was shown to be independent of solute concentration and period of usage.

Current research is focused on exploring a higher range of polymer surface densities and different choices of grafted polymer. Efforts are directed at optimizing CSP pervaporation membranes for increased selectivity as well as elucidating the mechanism of CSP pervaporation.

6. Nomenclature

A	membrane active area (cm^2)
$C_{b,i}$	molar concentration of component i in feed side bulk (mol/cm^3)
$C_{f,i}$	interfacial molar concentration of component i in feed (mol/cm^3)
$C_{i,0}$	initial feed tank concentration at start of pervaporation (mol/cm^3)
$C_{i,inp}$	molar feed concentration of component i at membrane inlet (mol/cm^3)
$C_{i,out}$	molar feed concentration of component i at membrane outlet (mol/cm^3)
$C_{mf,i}$	interfacial molar concentration of component i on feed side of membrane surface (mol/cm^3)
$C_{mp,i}$	interfacial molar concentration of component i on permeate side of membrane surface (mol/cm^3)
$C_{p,i}$	molar concentration of component i on permeate side (mol/cm^3)

$C_{pm,i}$	interfacial molar concentration of component i on permeate side (mol/cm ³)	$s_{p,i}$	partition coefficient between membrane and membrane surface on the permeate side for component i
$C_{T,feed}$	total feed concentration including all species (mol/cm ³)	t	pervaporation time (s)
d_h	inside diameter of the membrane tube (cm)	u	average flow velocity through membrane tube (cm/s)
D_i	solute diffusivity of component i in boundary layer (cm ² /s)	V	feed tank volume (cm ³)
D_w	diffusivity of water in air (cm ² /s)	V_0	feed tank volume at start of pervaporation (cm ³)
J_i	molar flux of component i through the membrane (mol/cm ² s)	$x_{b,i}$	mole fraction of component i in the feed
J_w	molar flux of water through the membrane (mol/cm ² s)	$x_{b,j}$	mole fraction of component j in the feed
k	permeability of the bulk solution through the membrane (cm ²)	$x_{b,o}$	mole fraction of organic component in the feed
$k_{f,i}$	tube-side mass transfer coefficient for the transport of component i through concentration boundary layer (cm/s)	$x_{p,i}$	mole fraction of component i in the permeate
$k_{m,i}$	mass transfer coefficient for the transport of component i through the membrane (cm/s)	$x_{p,j}$	mole fraction of component j in the permeate
$k_{ov,i}$	overall mass transfer coefficient of component i (cm/s)	$x_{p,o}$	mole fraction of organic component in the permeate
$k_{p,i}$	permeate-side mass transfer coefficient for component i (cm/s)	α	separation factor
L	total effective length of membrane (cm)	β	enrichment factor
M_i	molecular weight of component i (g/mol)	ρ_i	density of component i (g/cm ³)
N_p	total permeate flux through membrane (cm/s)	ρ_w	density of liquid water (g/cm ³)
N_w	water permeation flux expressed as liquid water flux (cm/s)	Δ	separation between polymer and solute in Hansen space, $\Delta = (\delta_d^2 + \delta_p^2 + \delta_h^2)^{1/2}$ (J/cm ³) ^{1/2}
P_i^s	saturation vapor pressure of component i (Pa)	ΔC_i	transmembrane concentration difference for component i (mol/cm ³)
Q	total volumetric flow through membrane feed side (cm ³ /s)	ΔC_w	transmembrane concentration difference for water (mol/cm ³)
Q_{inp}	volumetric flow rate at membrane inlet (cm ³ /s)	δ	concentration boundary layer thickness (cm)
Q_p	total permeate volumetric flow (cm ³ /s)	d_d	solubility parameter representing nonpolar forces (J/cm ³) ^{1/2}
Q_w	permeate volumetric flow rate for water (cm ³ /s)	δ_h	solubility parameter representing hydrogen bonding forces (J/cm ³) ^{1/2}
R	inside radius of membrane tube (cm)	δ_p	solubility parameter representing polar forces (J/cm ³) ^{1/2}
R_c	overall membrane resistance to convective flux of water (g/cm ² -s)	ΔP	transmembrane pressure (g/cm s ²)
R_d	overall membrane resistance to diffusive flux of water (g/cm ² -s)	μ	solution viscosity (g/cm s)
Re	Reynolds number	ν	kinematic viscosity of feed solution (cm ² /s)
R_i	overall membrane diffusive mass transfer resistance for component i (mol s/cm ⁴)	τ	membrane tortuosity
Sc	Schmidt number	θ	membrane thickness (cm)
$s_{f,i}$	partition coefficient between feed and membrane interface for component i		
Sh	Sherwood number		

Acknowledgements

The authors acknowledge the support of the National Science Foundation, the US Department of Energy, the UCLA Academic Senate and the UC Toxics Research and Teaching Program. The help of Professor Julius Glater is also acknowledged.

References

- [1] G.F. Tusel, H.E.A. Bruschke, Use of pervaporation in the chemical industry, *Desalination* 53 (1985) 327.
- [2] T. Kashiwagi, K. Okabe, K. Okita, Separation of ethanol from ethanol/water mixtures by plasma-polymerized membranes from silicone compounds, *J. Membr. Sci.* 36 (1988) 353.
- [3] A. Niemöller, H. Scholz, B. Götz, G. Ellinghorst, Radiation-grafted membranes for pervaporation of ethanol/water mixtures, *J. Membr. Sci.* 36 (1988) 124.
- [4] J. Redman, Pervaporation heading for a new horizons, *Chem. Eng. London* 669 (1990) 46.
- [5] M. Wesslein, A. Heintz, R.N. Lichtenthaler, Pervaporation of liquid mixtures through poly (vinyl alcohol) (PVP) membranes. II. The binary systems methanol/1-propanol and methanol/dioxane and the ternary system water/methanol/1-propanol, *J. Membr. Sci.* 51 (1990) 181.
- [6] M. Wesslein, A. Hwintz, R.N. Lichtenthaler, Pervaporation of liquid mixtures through poly (vinyl alcohol)(PVA) membranes I. Study of water containing binary systems with complete and partial miscibility, *J. Membr. Sci.* 51 (1990) 169.
- [7] H.L. Fleming, Consider membrane pervaporation, *Chem. Eng. Progr.* 88 (1992) 46.
- [8] J.Y. Lai, S. Li, K. Lee, Permselectivities of polysiloxaneimide membrane for aqueous ethanol mixture in pervaporation, *J. Membr. Sci.* 93 (1994) 273.
- [9] T. Sano, H. Yanagishita, Y. Kiyozumi, F. Mizukami, K. Haraya, Separation of ethanol/water mixture by silicalite membrane on pervaporation, *J. Membr. Sci.* 95 (1994) 221.
- [10] K.M. Song, W.H. Hong, Dehydration of ethanol and isopropanol using tubular type cellulose acetate membrane with ceramic support in pervaporation process, *J. Membr. Sci.* 123 (1997) 27–33.
- [11] C.L. Zhu, C.W. Yuang, J.R. Fried, D.B. Greenberg, Pervaporation membranes – A novel separation technique for trace organics, *Environ. Progr.* 2 (1983) 132.
- [12] J.P. Brun, C. Larchet, G. Bulvestre, B. Auclair, Sorption and pervaporation of dilute aqueous solutions of organic compounds through polymer membranes, *J. Membr. Sci.* 25 (1985) 55.
- [13] T.Q. Nguyen, K. Nobe, Extraction of organic contaminants in aqueous solutions by pervaporation, *J. Membr. Sci.* 30 (1987) 11.
- [14] B. Raghunath, S.T. Hwang, General treatment of liquid-phase boundary layer resistance in the pervaporation of dilute aqueous organics through tubular membranes, *J. Membr. Sci.* 75 (1992) 29.
- [15] T. Yamaguchi, S. Yamahara, S. Nakao, S. Kimura, Preparation of pervaporation membranes for removal of dissolved organics from water by plasma-graft filling polymerization, *J. Membr. Sci.* 95 (1994) 39.
- [16] J.G. Wijmans, A.L. Athayde, R. Daniels, J.H. Ly, H.D. Kamaruddin, I. Pinnau, The role of boundary layers in the removal of volatile organic compounds from water by pervaporation, *J. Membr. Sci.* 109 (1996) 135.
- [17] M.G. Liu, J.M. Dickson, P. Cote, Simulation of a pervaporation system on the industrial scale for water treatment. Part I. Extended resistance-in-series model, *J. Membr. Sci.* 111 (1996) 227.
- [18] J. Sheng, Separation of dichloroethane-trichloroethylene mixtures by means of a membrane pervaporation process, *Desalination* 80 (1991) 85.
- [19] P. Aptel, N. Challard, J. Cuny, J. Neel, Application of the pervaporation process to separate azeotropic mixtures, *J. Membr. Sci.* 1 (1976) 271.
- [20] M.S.K. Chen, G.S. Markiewicz, K.G. Venugopal, Development of membrane trimTM process for methanol recovery from CH₃OH/MTBE/C₄ mixtures, Membrane separations in chemical industries, *AIChE Symp.* 85(272) (1989) 82.
- [21] B.A. Farnand, Pervaporation as an alternative process for the separation of methanol from C₄ hydrocarbons in the production of MTBE and TAME, Membrane Separations in Chemical Industries, *AIChE Symp.* 85(272) (1989) 89.
- [22] J. Charpin, A.J. Burggraf, L. Cot, A survey of ceramic membranes for separations in liquid and gaseous media, *Ind. Ceram.* 11 (1991) 84.
- [23] M. Goldman, D. Fraenkel, G. Levin, A zeolite/polymer membrane for separation of ethanol–water azeotrope, *J. Appl. Polym. Sci.* 37 (1989) 1791.
- [24] S. Ulutan, T. Nakagawa, Separability of ethanol and water mixtures through PTMSP-silica membranes in pervaporation, *J. Membr. Sci.* 143 (1998) 275.
- [25] Y. Zhu, R.G. Minet, T.T. Tsotsis, A continuous pervaporation membrane reactor for the study of esterification reactions using a composite polymeric/ceramic membrane, *Chem. Eng. Sci.* 51(17) (1996) 4103.
- [26] Y. Zhu, H. Chen, Pervaporation separation and pervaporation–esterification coupling using crosslinked PVA composite catalytic membranes on porous ceramic plate, *J. Membr. Sci.* 138 (1998) 123.
- [27] S. Sakohara, F. Muramoto, T. Sakata, M. Asaeda, Separation of acetone/water mixture by thin acrylamide gel membrane prepared in pores of thin ceramic membrane, *J. Chem. Eng. Jpn.* 23 (1990) 40.
- [28] M. Chaimberg, Y. Cohen, Free radical graft polymerization of vinylpyrrolidone onto silica, *Ind. Eng. Chem. Res.* 30 (1991) 2534.
- [29] T. Browne, M. Chaimberg, Y. Cohen, Graft polymerization of vinyl acetate onto silica, *J. Appl. Polym. Sci.* 44 (1992) 671.
- [30] T. Okada, T. Matsuura, A new transport model for pervaporation, *J. Membr. Sci.* 59 (1991) 133–150.
- [31] T. Okada, T. Matsuura, Predictability of transport equations for pervaporation on the basis of pore-flow mechanism, *J. Membr. Sci.* 70 (1992) 163–175.
- [32] R.K. Tyagi, A.E. Fouda, T. Matsuura, A pervaporation model: membrane design, *Chem. Eng. Sci.* 90 (1995) 3105.
- [33] E. Bode, M. Busse, K. Ruthenberg, Consideration on Interface resistances in the process of permeation of dense membranes, *J. Membr. Sci.* 77 (1993) 69.
- [34] E. Matthiasson, B. Sivik, Concentration polarization and fouling, *Desalination* 35 (1980) 59.

- [35] V. Gekas, B. Hallstrom, Mass transfer in the membrane concentration polarization layer under turbulent crossflow. I. Critical literature review and adaption of existing Sherwood correlations to membrane operations, *J. Membr. Sci.* 30 (1987) 153.
- [36] H.H. Nijhuis, Removal of Trace Organics from Water by Pervaporation. A Technical and Economic Analysis, Ph.D. Dissertation, University of Twente, Enschede, The Netherlands, 1990.
- [37] C. Lipski, P. Côté, The use of pervaporation for the removal of organic contaminants from water, *Environ. Progr.* 9 (1990) 254.
- [38] H.O.E. Karlsson, G. Tragardh, Aroma compound recovery with pervaporation. Feed flow effects, *J. Membr. Sci.* 81 (1993) 163.
- [39] Van Krevelen D.W., *Properties of Polymers*, 3rd ed., Elsevier, New York, 1990.
- [40] C.M. Hansen, *The Three-dimensional Solubility Parameter and Solvent Diffusion Coefficient*, Danish Technical Press, Copenhagen, 1967.
- [41] Y. Cohen, J.-D. Jou, W. Yoshida, N. Bei, in: J.A. Wingrave (Ed.), *Oxide Surfaces*, Marcel Dekker, New York, 1998.
- [42] J.-D. Jou, Graft Polymerization and Application to Membrane Pervaporation, Ph.D. Dissertation, University of California, Los Angeles, CA, 1998.
- [43] Y. Cohen, High yield water-soluble polymer silica separation resins, US Patent 5 035 803 (1991).
- [44] M. Chaimberg, Y. Cohen, Kinetic modeling of free radical graft polymerization, *AIChE J.* 40 (1994) 294.
- [45] R.P. Castro, Y. Cohen, H.G. Monbouquette, Silica-supported polyvinylpyrrolidone filtration membranes, *J. Membr. Sci.* 115 (1996) 179.
- [46] T. Yamaguchi, S. Nakao, S. Kimura, Plasma-graft filling polymerization: preparation of a new type of pervaporation membrane for organic liquid mixtures, *Macromolecules* 24 (1991) 5522.
- [47] T. Yamaguchi, S. Nakao, S. Kimura, Design of pervaporation membrane for organic-liquid separation based on solubility control by plasma-graft filling polymerization technique, *Ind. Eng. Chem. Res.* 32 (1993) 848.
- [48] T. Yamaguchi, A. Tominaga, S. Nakao, S. Kimura, Chlorinated organics removal from water by plasma-graft filling polymerized membranes, *AIChE J.* 42 (1996) 892.
- [49] T. Yamaguchi, S. Nakao, S. Kimura, Evidence and mechanisms of filling polymerization by plasma-induced graft polymerization, *J. Polym. Chem. Ed.* 34 (1996) 1203.